Available online at www.sciencedirect.com
SCIENCE DIRECT®
Journal of Nuclear Materials 322 (2003) 1–14
journal of nuclear materials
www.elsevier.com/locate/jnucmat

Modeling of the non-monotonous viscoplastic behavior of uranium dioxide

F. Sauter [a,*], S. Leclercq [b]

[a] LEMTA/INPL, 2, avenue de la Forêt de Haye, 54504 Vandoeuvre cedex, France
[b] EDF/DRD MMC Branch, BP 1, Les Renardières, 77818 Moret sur Loing cedex, France

Received 14 September 2002; accepted 14 May 2003

Abstract

In order to evaluate the stress level during pellet cladding mechanical interaction (PCMI), Electricité de France is involved in a large program of investigation of the mechanical properties of both fuel pellets and claddings. In this paper, we focus on the mechanical behavior of uranium dioxide. These pellets exhibit a yield point during strain hardening tests and sigmoïdal creep curves, that is inflection points characteristic of a non-monotonous viscoplastic flow in the first stages of the tests. Inspired by Alexander and Haasen's work upon single crystal silicon, we develop a dislocation-based model that is able to describe the viscoplasticity of uranium dioxide in the range of temperature and stress of the PCMI. After developing this model, we introduce it into the Pilvin's polycrystalline approach. The self-consistency of the polycrystalline approach in the case of a non-monotonous viscoplastic flow is demonstrated in an independent article.

PACS: 83.60.La; 81.40.Lm; 46.35.+z

1. Introduction

Nearly 80% of electricity production in France relies on nuclear power. Seasonal variations of the power requirement, which cannot be handled by non-nuclear production, must be translated to variations of the reactor power delivery. During power transitions, the pellets of uranium dioxide encounter the zirconium alloy cladding and triggers strain in the latter. For these pressured light water reactors, the temperature in the center of the pellet can reach 1600 °C whereas it is close to 900 °C near the cladding. Thus as the melting temperature is roughly 3000 K, viscoplastic flow is likely to appear in the hot part of the pellet. The viscoplasticity will relax a fraction of the stress in the pellet, hence in the pellet cladding interaction zone. Therefore, the assessment of stress during pellet cladding mechanical interaction (PCMI) requires the knowledge and the modeling of the viscoplastic flow of uranium dioxide.

In normal conditions, that is when the power requirement is constant, steady state laws are sufficient to describe creep phenomena and the evolution of the diameter of the pellet. In the case of a power ramp, a finite element method study requires a complete constitutive equation. Leclercq [1] has proposed a phenomenological model of the viscoplastic flow based on a hardening multiplication viscosity law, which simply describes stress relaxation, hardening and creep (stages I and II). In that paper, the law was identified for the case of uranium dioxide and Leclercq proposed a model of the effect of the variation of porosity. Note that, for the sake of simplicity, the pellets used for the identification had a monotonous viscoplastic flow whereas standard pellets exhibit two inflection points at the beginning of the viscoplastic flow during stain hardening tests (see Fig. 1(a)). This phenomenon, called 'yield point', is due to a cascade of dislocations, typical for low dislocation

* Corresponding author.
E-mail addresses: fabien.sauter@cea.fr (F. Sauter), sylvain.lerclercq@edf.fr (S. Leclercq).

0022-3115/$ - see front matter © 2003 Elsevier B.V. All rights reserved.
doi:10.1016/S0022-3115(03)00276-9

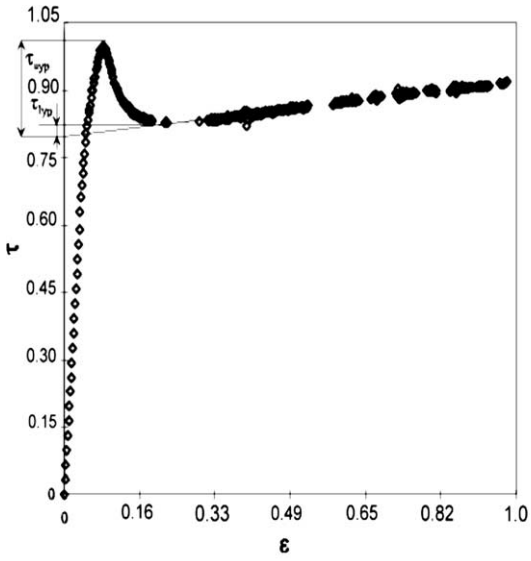

(a) Normalized strain hardening curve

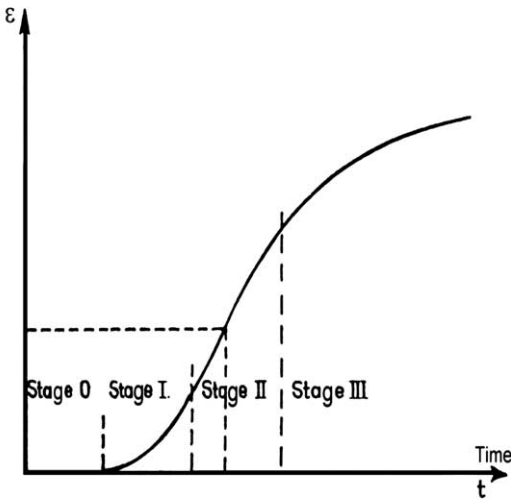

(b) Normalized creep curve

Fig. 1. Characteristic behavior of materials exhibiting yield points.

density materials. The corollary of the so-called yield point is a sigma-shaped creep curve, which amounts to a significant increase of both dislocation density and velocity (see Fig. 1(b)). The sigma-shaped creep curve is the subject of this paper.

First, we recall the main features of the surroundings of the pellets so as to understand the structural and material behavior of uranium dioxide. As the yield point has been widely studied for single crystal silicon, we start from Alexander and Haasen's model well known for its ability to describe non-monotonous viscoplastic flow but whose major weaknesses are the multiplication law for dislocations and the internal stress expression. Thus we develop a multiplication law that correctly describes the material behavior. Afterwards, we extend the model into a polycrystalline approach.

While macroscopic fits are not absolute evidence of the behavior of a material, we have tried, as far as possible, to couple these fits with observations of the microstructure of uranium dioxide.

For the sake of intellectual property, the numerical value of the stress and strains will be normalized.

2. Mechanical environment

2.1. Structural effects

During PCMI the temperature is likely to be close to 1600 °C in the center of the pellet and 900 °C at its border. The boundary conditions of the thermal problem encounter a diabolo shape (see Fig. 2(a)). Due to the huge temperature gradient (the radius of the pellet is about 4 mm), the thermal stress becomes very high. Since the uranium dioxide is brittle in the cold area, the pellet bursts out into fragments (see Fig. 2(b)). Note that the fragmentation is both radial and axial.

2.2. Crystallography

Uranium dioxide is a partially ionic solid. Its structure is called fluorite, which is the stable phase of uranium dioxide for any temperature. Crystalline uranium dioxide is made of U^{4+} and O^{2-}. The oxygen ions are arrayed in a simple cubic lattice and the uranium ions form a fcc sublattice. Note that the unoccupied interstitial positions in the body centers of the small cubes do not contain uranium ions.

The ionic structure triggers a major consequence upon dislocations which are represented by two semi-planes in order not to disturb the electric neutrality. Assuming a perfectly ionic solid, Lefebvre [2] calculated the stacking fault energy for UO_2 and found that since the value is very high, glissile dissociation is very unlikely. Since screw dislocations have no electric charge, their motion is faster hence hereafter we only consider the corner dislocations in our modeling (see [3]).

The primary glide system is $\langle 1\,1\,0\rangle\{0\,0\,1\}$, the critical resolved shear stress (CRSS) is nearly half that of the system $\langle 1\,\bar{1}\,0\rangle\{1\,1\,0\}$. If this system is active, dislocation networks are created upon two directions. Eventually interactions with the plane $\{1\,1\,1\}$ trigger an hexagonal network. In the range of temperature and stress of this study, there are five independent slip planes. The crystallography of uranium dioxide is very sensitive to both irradiation and stoichiometry control.

The influence of an excess of oxygen has been studied since it eases the sintering of the pellet. The third digit of

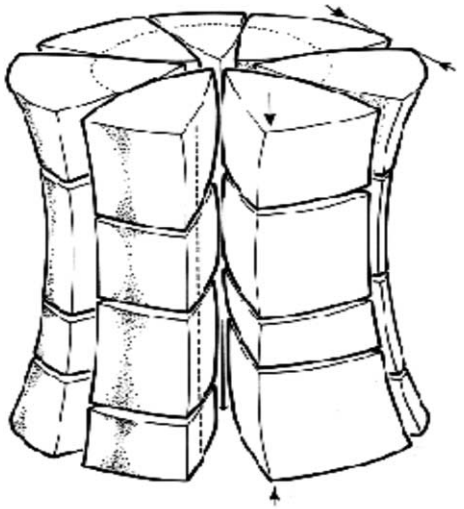

(a) Schematic representation of the fragmentation and the diabolo effect.

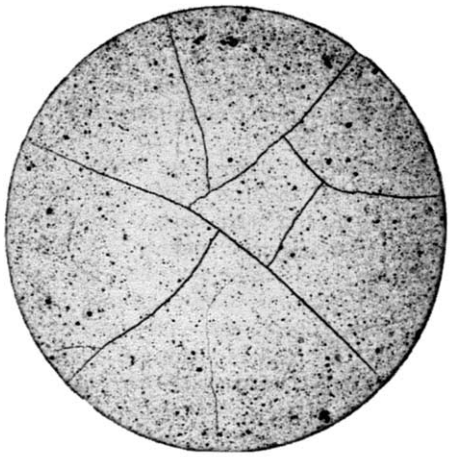

(b) Real fragmentation of a pellet.

Fig. 2. Fragmentation of a pellet due to the thermal gradient.

the stoichiometric ratio O/U has a very large influence on the strain rate, at 1500 °C the strain rate of a pellet with a stoichiometric ratio of 2.001 is 1200 times bigger than the strain rate of the stoichiometric pellet (see [4]).

Irradiation, that is neutron flux $\dot{F}$, is likely to enhance the viscoplastic flow of uranium dioxide. Moreover there exists an irreversible strain rate $\dot{\varepsilon}^{\mathrm{irr}}$, which is a function of the absorbed irradiations. Hence the anelastic strain is written:

$$\dot{\varepsilon}^{\mathrm{an}} = \dot{\varepsilon}^{\mathrm{irr}} + \dot{\varepsilon}^{\mathrm{vp}}_{\dot{F}=0}(1 + c\dot{F}), \tag{1}$$

where $\dot{F}$ is the number of fissions per cm^3 per s (see [5]).

2.3. Viscoplastic mechanisms

In the range of temperature and stress of the PCMI, according to Ashby and Frost [6], see the clear grey rectangle of Fig. 3(a), the strain rate is controlled by dislocation motion. When the temperature is greater than $T_{\mathrm{m}}/2$, grain boundary diffusion becomes noticeable.

Numerous authors have proposed steady state creep laws for specific mechanisms. Let us summarize the main ones. In the case of vacancy diffusion, the strain rate is a

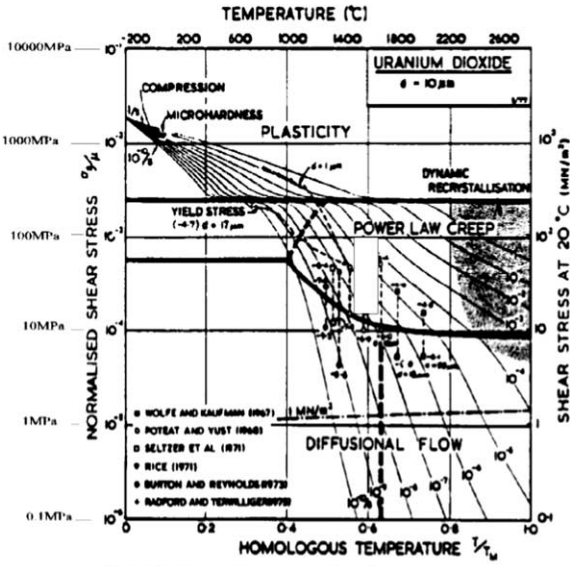

(a) Deformation mechanisms map (Ashby [6]).

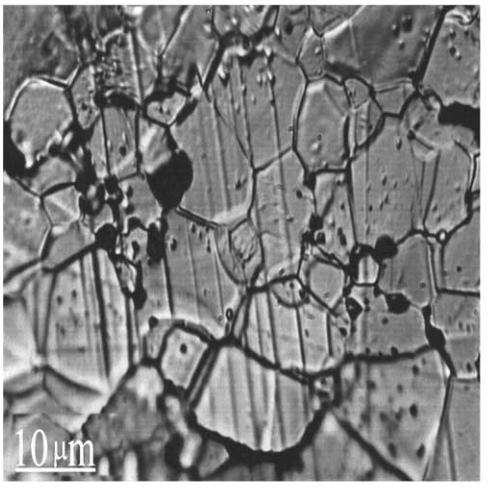

(b) SEM picture of a UO_2 pellet deformed at 6% (Vivant-Duguay [29]).

Fig. 3. Deformation mechanism and cavities coalescence [6,29].

linear function of the stress and depends on the grain size:

$$\dot{\varepsilon}^{vp} = \frac{B}{d^{\alpha}}\sigma \exp\left(-\frac{Q}{RT}\right), \tag{2}$$

where d is the grain size, Q is the activation energy of vacancy diffusion, B is a constant and $\alpha = 2$ or 3 dependent on whether the diffusion takes place in the bulk or in the grain boundary (see [7,8]).

In the case of dislocation motion, the strain rate is independent of the grain size but it is a non-linear function of the stress:

$$\dot{\varepsilon}^{vp} = B_m \sigma^n \exp\left(\frac{-Q_{vol}}{RT}\right), \tag{3}$$

where Q_{vol} is the activation energy of vacancy diffusion in the bulk. In the Weertman's model, based on dislocation annihilation $n = 4.5$. Nevertheless, these models rely on descriptions which sometimes have not been observed. Thus, they may not be satisfying.

Another weakness of these descriptions is the statement of macroscopic threshold between mechanisms. In the case of a polycrystal, it is much more realistic to consider that in some grains the strain rate is controlled by dislocation motion whereas elsewhere, for lower stress level, vacancy diffusion is predominant. Ashby and Verrall [9] have proposed a versatile model which describes the strain rate as a weighted sum of the former mechanisms:

$$\dot{\varepsilon}^{L}_{diff} = \frac{\alpha_l \sigma}{Td^2} \exp\left(-\frac{Q_{vol}}{RT}\right), \tag{4}$$

$$\dot{\varepsilon}^{B}_{diff} = \frac{\alpha_l r \sigma}{Td^3} \exp\left(-\frac{Q_{gb}}{RT}\right), \tag{5}$$

$$\dot{\varepsilon}_{dislo} = \frac{\alpha_s \sigma^n}{T} \exp\left(-\frac{Q_{vol}}{RT}\right), \tag{6}$$

where α_l and α_s are parameters to be identified on macroscopic tests.

2.4. Damage evidences

Scanning electron microscopy (SEM) pictures (see Fig. 3(b)), indicate the coalescence of vacancies near the grain boundary which gives rise to cavities. Thus the efficient section is reduced, that is damage occurs during the strain-hardening test. The elastic properties are assumed to be linear decreasing functions of a scalar variable D taking into account mechanical damage effects, for instance $E^u = E_0(1 - D)$ where E^u is the Young's modulus and E_0 is the Young's modulus at the beginning of the test. We do not discuss the effects of damage on the viscoplastic strain rate, nevertheless we quote Lemaitre and Chaboche [10] and Kachanov [11] who have proposed viscoplastic models coupled with damage functions.

Table 1
Estimation of the evolution of the Young's modulus due to damage [28]

Pre-strain (%)	Estimation of the Young's modulus (GPa)
0	229
4.47	164
6.50	163
7.02	158

We propose a first estimation of the damage in the case of UO_2 using microacoustic measurements (see [12]). In Table 1, we give the estimated Young's modulus for different strain levels. At first sight, it appears that damage cannot be disregarded and should be further studied. Unfortunately, discriminant tests are not numerous enough to do so. Three points bending test and inverse method identification are required. Hereafter, damage will be assumed to be an increasing linear function of the viscoplastic strain.

3. Modeling of the non-monotonous viscoplastic flow, dislocation based-model

Most of the pellets formerly used for the study of uranium dioxide do not exhibit a non-monotonous viscoplastic flow, whereas industrial pellets do. Sigma creep curves and yield point are characteristic of this kind of viscoplastic behavior. This feature has been widely studied for single crystal silicon and NaCl salt. It is common to many materials where the dislocation density is very low and the velocity of the dislocation is controlled by Peierls' forces. Note that point defects can also pin dislocations and trigger yield points.

We are aware that there is a lack of information on the microstructure. Moreover the correct fit of our experiments by macroscopic models is by no way an evidence of the existence of a phenomenon. Nevertheless, our results are excellent over a wide range of temperature and stress ([950; 1600 °C] and [15; 250 MPa] respectively) and our interpretations are consistent with the literature.

Hereafter, we start by recalling the Alexander and Haasen's model with its advantages and drawbacks, highlighting its assumptions. Then we propose modifications of some features and also introduce, according to Ashby and Verrall, a diffusion mechanism that takes into account the grain boundary sliding assuming superposition of the viscoplastic flows. Finally, we present the limits of this approach and introduce our development of a polycrystalline framework.

3.1. Description of the experimental data

The equipment had been designed by the *Commissariat à l'Energie Atomique* (CEA) and Dr Mocellin's team performed the mechanical tests on an Instron 1185 with a maximum load of 10 tons. The pellets are tested in creep, stress relaxation and strain hardening test. The load type is compression and the tests are strain-controlled. In order to avoid any stoichiometry change, the oven atmosphere is regulated with (95%Ar, 5%H2) at 50 l/h. The average moisture level is 0.02% in volume. Note that a very large experimental program was performed by the CEA in order to model the steady state creep of uranium dioxide. In particular, Dherbey et al. [13] used transmission electron microscopy (TEM) and SEM analysis to correlate microstructure to macroscopic mechanical behavior. The temperature is controlled by several thermocouples.

We made an approximation concerning the shape of the pellet. On Fig. 4, one can see a pellet deformed at 16%. Due to friction on the top and the bottom sides, the pellet has a barrel shape. On Fig. 4(b), we illustrate the consequence of the assumption of stress homogeneity showing that the strain is slightly over evaluated.

In order to specify the tests for identification, especially the strain rate, we use a previous study performed by Diard with the FEM code *Zébulon* at the *Centre des Matériaux*, Evry. This modeling describes one sixteenth of the pellet and the cladding, which undergo a power ramp like a temperature load. There is an increase of the pellet diameter, then the pellet imposes its strain to the cladding. After a significant increase of the stress, stress relaxation occurs due to viscoplastic flow. The constitutive equation used for the pellet is a multiplicative-viscosity hardening, see Leclercq [1] with a specific model for the cladding (see [14]). The maximum stress is about 250 MPa and $\dot{\varepsilon}_{\max} \simeq 10^{-5}\ \mathrm{s}^{-1}$. Hence the chosen strain rate for our tests.

3.2. Description of the model

3.2.1. Description of the Alexander and Haasen's model

This model includes a single dislocation density [15]. This strong assumption must be explained. It was shown by etch pit at the early stage of the viscoplastic flow that most of the dislocations belong to the primary slip plane and that the dipoles or multipoles are invisible. Consequently, the measured dislocation density is closer to the density of mobile dislocations than the total density of dislocations.

Let us now recall the constitutive equations:

$$v = v_0 \left(\frac{\tau^*}{\tau_0} \right)^m \exp\left(-\frac{\Delta H_0}{RT} \right), \tag{7}$$

$$\dot{\gamma} = \frac{\dot{\tau}}{M_a} + \mathtt{b}\rho v, \tag{8}$$

$$\tau^* = \max(0; \tau - \tau_i), \tag{9}$$

$$\dot{\rho} = K\rho v \tau^*, \tag{10}$$

where v, $\mathtt{b}$, ΔH_0, ρ, τ^*, τ_i, M_a are respectively the velocity of dislocations, the magnitude of the Burgers' vector, the free enthalpy, the density of dislocations, the effective stress, the internal stress and the stiffness of the test

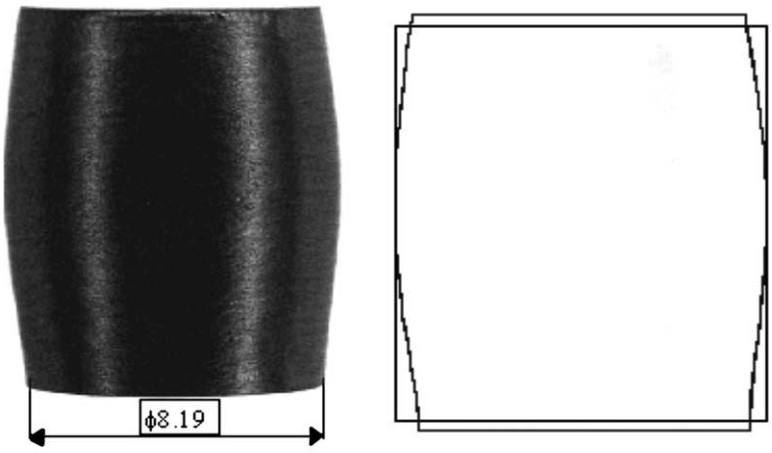

(a) Uranium dioxide pellet deformed at 16% (Vivant-Duguay [29]).

(b) Assumption of stress homogeneity.

Fig. 4. Barrel shape after compression tests [29].

machine (equivalent to an apparent shear modulus). Taking into account the machine and the explored range of temperature, the value of M_a largely differs from μ, the shear modulus ($M_a \simeq \mu/10$ from our identifications which is consistent with the remarks of Rabier and George [16]). In the literature, one finds $1 \leqslant m \leqslant 2$.

The expression for the effective stress is:

$$\tau_i = \frac{\mu b}{2\pi(1-\nu)}\sqrt{\rho}, \tag{11}$$

where one recognizes the signature of corner dislocations.

Note that the dislocation density still grows if $\dot{\tau} \leqslant 0$, i.e. $\dot{\varepsilon} \leqslant \dot{\varepsilon}^{vp}$, as it depends on the effective stress τ^*. Moulin et al. [17] called this phenomenon 'overshoot'. It means that after the threshold $\tau \geqslant \tau_i$, the dislocations become mobile and triggers a significant growth of the viscoplastic strain rate, which in the case of yield point is even larger than $\dot{\varepsilon}$. In this model the representative elementary volume is a set of grains of the same orientation, that is one considers a polycrystal of a single slip system. The only crystallographic information lays in the Burgers' vector.

One major advantage of this model is its ability to predict and to estimate the stress at the upper yield point and lower yield point, respectively τ_{UYP} and τ_{LYP}. Eq. (9) can be written the following:

$$\tau = \tau^* + A\sqrt{\rho}, \tag{12}$$

inverting Eq. (7), (12) becomes, with $B(T) = \exp[-\Delta H_0/RT]$:

$$\tau = \tau_0\left(\frac{\dot{\gamma} - \frac{\dot{\tau}}{M_a}}{\mathfrak{b}\rho v_0 B(T)}\right)^{1/m} + A\sqrt{\rho}. \tag{13}$$

The yield point is a local extremum of the stress curve versus strain:

$$\tau_{YP} \text{ is such that } \left(\frac{\partial\tau}{\partial\gamma}\right)_{\dot{\gamma}} = 0. \tag{14}$$

Let us first focus on τ_{LYP}. Haasen [1] writes

$$\tau = \tau(\gamma,\rho) \Longleftrightarrow \dot{\tau} = \frac{\partial\tau}{\partial\rho}\dot{\rho} + \frac{\partial\tau}{\partial\gamma}\dot{\gamma}$$

and assumes $(\partial\tau/\partial\rho)_{LYP} = 0$. Hence, the density of dislocations at this specific point is

$$\rho_{LYP} = \left(\frac{2}{Am}\right)^{2m/(m+2)}\left[\frac{\dot{\gamma}\tau_0^m}{v_0\mathfrak{b}\exp\left(-\frac{\Delta H_0}{RT}\right)}\right]^{2/(m+2)}. \tag{15}$$

Then, he introduces this result in Eq. (13) and obtains:

$$\tau_{LYP} \propto \dot{\gamma}^{1/(m+2)}\exp\left(\frac{\Delta H_0}{(m+2)RT}\right). \tag{16}$$

Note that this stress expression is independent of the initial dislocation density and of the kinetics of dislocation multiplication. At the upper yield point, Haasen settles that $(\partial\tau/\partial\rho)_{UYP} \neq 0$ and obtains an expression analogous to Eq. (16): [2]

$$\tau_{UYP} \propto \frac{\dot{\gamma}^{1/n}}{\rho_{UYP}}\exp\left(\frac{\Delta H_0}{nRT}\right). \tag{17}$$

We identify the parameters of the model by creep, relaxation and strain hardening tests performed on uranium dioxide for temperature between 950 and 1600 °C and stress included in [15; 250 MPa]. Our simulations indicate that the dislocation density at the UYP can be approximated by ρ_0. Moulin et al. [17] note the value of n is a little bit lower than $m+2$. n appears in Eq. (17).

These simulations are gathered on the graphs shown on Fig. 5 where we have compared the estimated value of the yield point with the measurement of these specific stresses on our tests. There is a good agreement between the model and the measurements.

Nevertheless, the value of m ($\approx$9.3) differs from the one found in the literature for silicon ($1 \leqslant m \leqslant 2$). This means that UO_2 is much less viscous than silicon at high temperature. If one sets a model like $\sigma_{UYP} \propto \dot{\varepsilon}^{1/\alpha}$, α is close to 17, which means according to Guérin [19] that the behavior of uranium dioxide tends to be more plastic than viscous.

3.2.2. Limits of the AH model

The AH model gives predictions of the stress at the yield point in good agreement with experimental data. The yield point stands for the dependency of the dislocation velocity on the effective stress and the multiplication law. Nevertheless, the AH model exhibits several limitations:

(1) The multiplication law is very simple since it does not take into account annihilation.
(2) We have justified the assumption of a single dislocation variable ρ at the early stages of plastic deformation. As we wish to identify the viscoplastic behavior of UO_2 up to $\dot{\varepsilon}^{vp} = 6.5\%$ it is necessary to use a more accurate description.

[1] One states that $\partial_T\rho_{m,ly} \simeq 0$. Note that Omri et al. [18] disagree with this and show that $\rho_{m,ly}$ varies as a function of the temperature so that the effective stress τ^*_{LYP} is closer of τ_{LYP} than of its prediction using the AH model ($\tau^*_{LYP} \simeq \tau_{LYP}/(m+2)$, where $1 \leqslant m \leqslant 2$).

[2] Lower yield point (LYP).

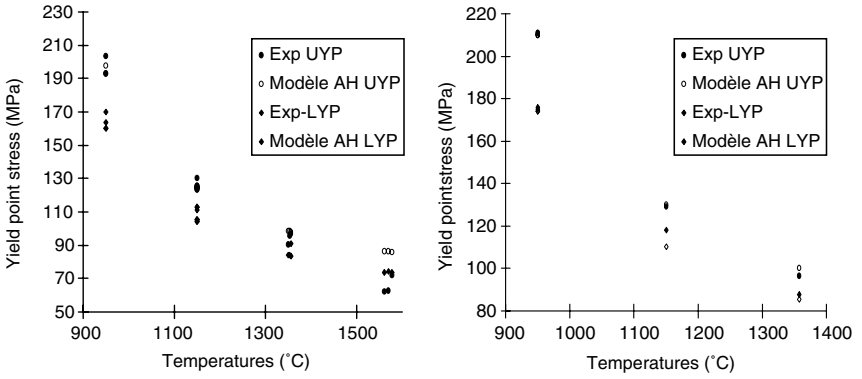

(a) $\dot{\varepsilon} = 2.0E-5\,\mathrm{s}^{-1}$ (b) $\dot{\varepsilon} = 6.5E-5\,\mathrm{s}^{-1}$

Fig. 5. Temperature dependence of the yield point stress for several strain rates.

(3) It has been shown with numerical identification that the expression of the internal stress is inaccurate.
(4) At high temperature and low stress level, according to the deformation mechanism map of Chapron et al. [5], the diffusion mechanism can become significant.

3.2.3. Description of our alternative model

To solve limitation 1, we have used the model given by Estrin and Mecking [20] where we disregard the term related to point defect versus dislocations interactions:

$$\dot{\rho} = \left(k_1\sqrt{\rho} - k_2(\dot{\gamma}^{\mathrm{vp}}, T)\rho\right)\dot{\gamma}^{\mathrm{vp}}. \tag{18}$$

The constant k_1 takes into account the hardening due to dislocation interactions and k_2 is the annihilation term of the model. Note that this phenomenon is thermally activated, see equation column 1 line 4 in Table 2.

To solve limitation 2, we refer once again to Kubin and Estrin, who developed a multiplication model using a system of two coupled differential equations: one for the mobile dislocation density ρ_{m}, one for the forest dislocation density ρ_{f}:

$$\frac{\mathrm{d}\rho_{\mathrm{m}}}{\mathrm{d}\varepsilon^{\mathrm{vp}}} = M_{\mathrm{T}}\left(-k_1\sqrt{\rho_{\mathrm{f}}} - k_3\rho_{\mathrm{m}} + k_4\frac{\rho_{\mathrm{f}}}{\rho_{\mathrm{m}}}\right), \tag{19}$$

$$\frac{\mathrm{d}\rho_{\mathrm{f}}}{\mathrm{d}\varepsilon^{\mathrm{vp}}} = M_{\mathrm{T}}\left(k_1\sqrt{\rho_{\mathrm{f}}} - k_2\rho_{\mathrm{f}} + k_3\rho_{\mathrm{m}}\right), \quad k_i \geqslant 0, \ \forall i. \tag{20}$$

Compared to Eq. (18), there is an additional coupling term taking into account the immobilization of some mobile dislocations k_3. Concerning forest dislocations they can be unpinned and become mobile (k_4). M_{T} is the Taylor's factor. According to Estrin, the viscoplastic strain rate is given by:

$$\dot{\varepsilon}^{\mathrm{vp}} = \zeta\rho_{\mathrm{m0}}\left(\frac{\sigma}{\sigma_0}\right)^m XY^{-m/2}, \tag{21}$$

where

$$X = \frac{\rho_{\mathrm{m}}}{\rho_{\mathrm{m0}}}, \quad Y = \frac{\rho_{\mathrm{f}}}{\rho_{\mathrm{f0}}},$$
$$\zeta = \exp\left[-\frac{\Delta H_0 * (1 - pq(\tau/\tau_{\mathrm{i}})^{\mathrm{p}}}{RT}\right] \quad \text{and} \quad \rho_{\mathrm{m0}}$$

is the initial density of mobile dislocations. Hence the previous equation can be written:

$$\dot{\varepsilon}^{\mathrm{vp}} = \zeta\rho_{\mathrm{m}}\left(\frac{\sigma}{\sigma_0\sqrt{Y}}\right)^m. \tag{22}$$

Table 2
Differing equations of the AH-like models

AH model (1 i.v.)	AH model (2 i.v.)	AH model (2 i.v.) + gbs
$\frac{\partial\rho}{\partial\dot{\gamma}^{\mathrm{vp}}} = \left(c_1\sqrt{\rho} - c_2(\dot{\varepsilon}, T)\rho\right)$	$\frac{\mathrm{d}X}{\mathrm{d}\varepsilon^{\mathrm{vp}}} = q\left(-c_1\sqrt{Y} - c_3X + c_4\frac{Y}{X}\right)$	$\frac{\mathrm{d}X}{\mathrm{d}\varepsilon^{\mathrm{vp}}} = q\left(-c_1\sqrt{Y} - c_3X + c_4\frac{Y}{X}\right)$
$\dot{\gamma}^{\mathrm{vp}} = \rho\mathfrak{b}v$	$\frac{\mathrm{d}Y}{\mathrm{d}\varepsilon^{\mathrm{vp}}} = \left(c_1\sqrt{Y} - c_2Y + c_3X\right)$	$\frac{\mathrm{d}Y}{\mathrm{d}\varepsilon^{\mathrm{vp}}} = \left(c_1\sqrt{Y} - c_2Y + c_3X\right)$
$c_2(\dot{\varepsilon}, T) = c_{20} * \exp\left(-\frac{\Delta H_0*(1-pq(\lvert\tau(\dot{\varepsilon})\rvert/\tau_{\mathrm{i}})^{\mathrm{p}}}{nRT}\right)$		$\dot{\varepsilon}_d^{\mathrm{vp}} = \zeta\rho_{\mathrm{m}}\left(\frac{\sigma-\sigma_{\mathrm{i}}}{\sigma_{\mathrm{i}}}\right)^m$
		$\dot{\varepsilon}_L^{\mathrm{vp}} = \frac{\alpha^*\sigma}{d^2}\exp\left(-\frac{\Delta H_0}{RT}\right)$
		$\dot{\varepsilon}_{\mathrm{gbs}}^{\mathrm{vp}} = \frac{\alpha^*\sigma r}{d^3}\exp\left(-\frac{\Delta H_B}{RT}\right)$
$\dot{\varepsilon}^{\mathrm{vp}} = \frac{\dot{\gamma}^{\mathrm{vp}}}{M_{\mathrm{T}}}$, $M_{\mathrm{T}} = 3.06$	$\dot{\varepsilon}^{\mathrm{vp}} = \zeta\rho_{\mathrm{m}}\left(\frac{\sigma-\sigma_{\mathrm{i}}}{\sigma_{\mathrm{i}}}\right)^m$	$\dot{\varepsilon}^{\mathrm{vp}} = \dot{\varepsilon}_d^{\mathrm{vp}} + \dot{\varepsilon}_{\mathrm{gbs}}^{\mathrm{vp}} + \dot{\varepsilon}_L^{\mathrm{vp}}$

This equation is an Orowan's law ($\dot{\gamma} = \mathtt{b}\rho_{\mathrm{m}} v$) with:

$$v = \frac{\zeta}{\mathtt{b}}\left(\frac{\sigma}{\sigma_0\sqrt{Y}}\right)^m = \frac{\zeta}{\mathtt{b}}\left(\frac{\sigma}{\sigma_{\mathrm{i}}}\right)^m. \tag{23}$$

This similarity strongly emphasizes the fact that it is a dislocation-based model.

The introduction of X and Y allows to write the system as:

$$\frac{\mathrm{d}X}{\mathrm{d}\varepsilon^{\mathrm{vp}}} = q\left(-c_1\sqrt{Y} - c_3 X + c_4\frac{Y}{X}\right), \tag{24}$$

$$\frac{\mathrm{d}Y}{\mathrm{d}\varepsilon^{\mathrm{vp}}} = \left(c_1\sqrt{Y} - c_2 Y + c_3 X\right), \tag{25}$$

with $q = \rho_{\mathrm{f}0}/\rho_{\mathrm{m}0}$.

Keeping in mind that the concept of effective stress is the crux of the Alexander and Haasen model (AH model), we modify the AH model introducing the distinction between mobile and forest dislocations in the multiplication law (Eqs. (24) and (25)) and the concept of effective stress in the viscoplastic strain rate of Eq. (22) [21]:

$$\dot{\varepsilon}^{\mathrm{vp}} = \zeta\rho_{\mathrm{m}}\left(\frac{\sigma - \sigma_{\mathrm{i}}}{\sigma_{\mathrm{i}}}\right)^m. \tag{26}$$

Regarding limitation 3, we refer to Moulin et al. [17], who introduced a corrective factor α on the internal stress to improve the fit with experimental data (see Eq. (28)) where d is the average grain size. As the mean free path is maximized by the grain size, like Kim et al. [22], we introduce a corrective factor K_{HP} in the expression of the internal stress. This dependency amounts to a Hall–Petch type law.

Finally, for limitation 4, according to Ashby and Verrall [9], we add a viscoplastic strain rate related to vacancy diffusion at the grain boundary.

Afterwards, we write and identify three models. The first one consists in a AH model with a multiplication law including a term related to annihilation (AH model 1 internal variable). The second one includes the Kubin and Estrin's differential system and the viscoplastic strain rate from Eq. (26). The third one includes all the features of the latter plus a term related to grain boundary sliding.

Hereafter we recall the common Eqs. (27)–(30) of these models. In Table 2, one finds the equations that differ. The parameters of the models were identified over the range of temperature [950; 1600 °C] and in the range of stress of [15; 250 MPa]. The 9 mechanical tests are presented on Fig. 6 and in Table 5. The value of the parameters are given in Table 4. Fig. 6(a)–(e) are strain hardening tests with stress relaxation steps and Fig. 6(f) is a creep test. In order to assess the stress relaxation kinetics, we decided to draw the stress versus time. On Fig. 7, one can see the comparison between the experiments and the simulation of the tests with the identified models:

$$\tau^* = \max(0; \tau - \tau_{\mathrm{i}}), \tag{27}$$

$$\tau_{\mathrm{i}} = \frac{\alpha\mu\mathtt{b}}{2\pi(1-\nu)}\sqrt{\rho} + \frac{K_{\mathrm{HP}}}{\sqrt{d}}, \quad \alpha = 1.48, \ \ \nu = 0.316, \tag{28}$$

$$v = v_0\left(\frac{\tau^*}{\tau_0}\right)^m \exp\left(-\frac{\Delta H_0 * (1 - pq(\tau(\dot{\varepsilon})/\tau_{\mathrm{i}})^{\mathrm{p}}}{RT}\right), \tag{29}$$

$$\zeta = \exp\left(-\frac{\Delta H_0 * (1 - pq(\tau/\tau_{\mathrm{i}})^{\mathrm{p}}}{RT}\right). \tag{30}$$

3.3. Discussion

The analysis of Figs. 6 and 7 indicates that at low temperatures and high stress, the AH-like model with a single dislocation density variable includes the necessary features to describe the viscoplastic behavior of uranium dioxide. But, as the temperature increases, the use of two dislocation densities becomes necessary. Finally, at high temperature and low stress, the relaxation kinetics, i.e. the viscoplastic flow is better described by a vacancy diffusion model. These results agree perfectly with the limits of the original AH model and with the extensions we have proposed.

Note that the present work is also consistent with the former studies on viscoplastic mechanisms of uranium dioxide at high temperature, which use one dislocation-based mechanism and the Coble's diffusion based mechanism, for instance Chapron et al. [5]. The yield point is only observed in the early stages of strain hardening tests, which means that a well-chosen pre-strain can avoid this phenomenon for the subsequent loads [16]. Finally, the comparison of the model with the experimental data is in good agreement with the studies on single crystal silicon, on which Alexander and Haasen developed their model. The features of this model allow the description of both the yield point and the sigma creep curves (see Figs. 1(b) and 6(f)). This discussion confirms that the concept of these models are in good agreement with the mechanical behavior we observed.

Note that there is no experimental evidence of grain boundary sliding, the good fit of a model not being a proof of physical meaning but rather an indication, especially when the number of adjustable parameters is large. However, we have managed to describe numerically the viscoplastic behavior of UO_2 on the range of temperature [950; 1600 °C] for stress from 15 to 250 MPa.

Although all of our reflections are based on the structure of uranium dioxide, no crystallographic information is mentioned except the Burgers' vector. Hence, it is difficult to extrapolate to large deformation due to the

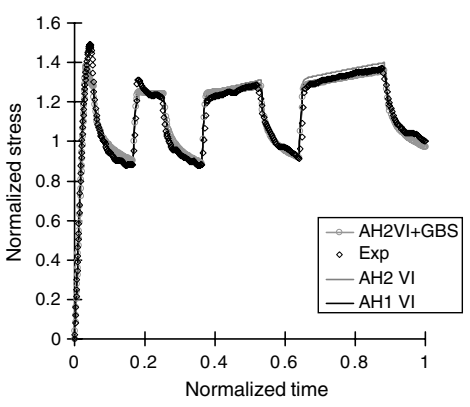

(a) $T = 950C$, $\dot{\varepsilon} = 1.45E-5\,\mathrm{s}^{-1}$

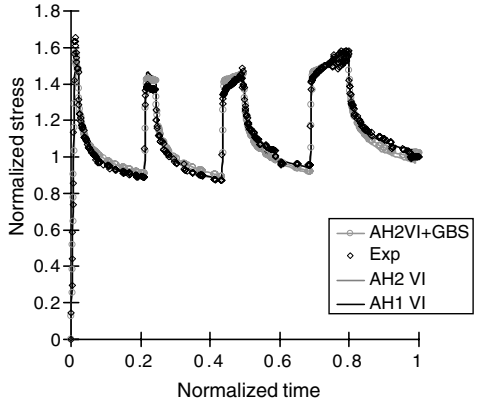

(b) $T = 950C$, $\dot{\varepsilon} = 6.24E-5\,\mathrm{s}^{-1}$

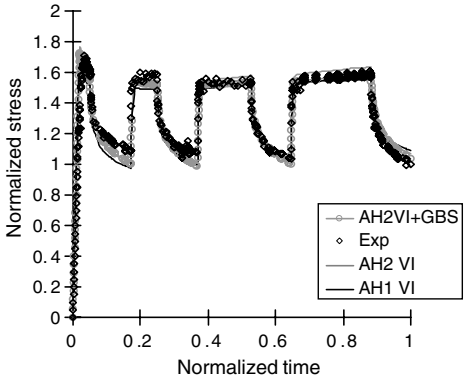

(c) $T = 1150C$, $\dot{\varepsilon} = 1.60E-5\,\mathrm{s}^{-1}$

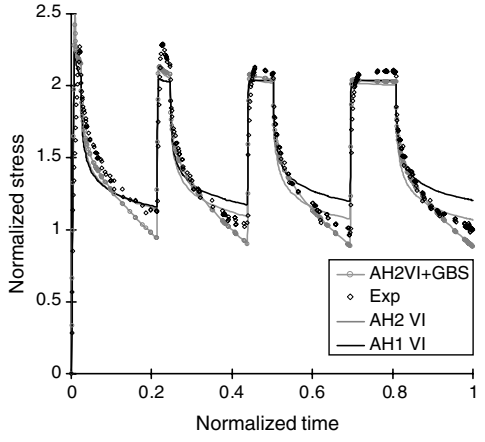

(d) $T = 1348C$, $\dot{\varepsilon} = 5.68E-5\,\mathrm{s}^{-1}$

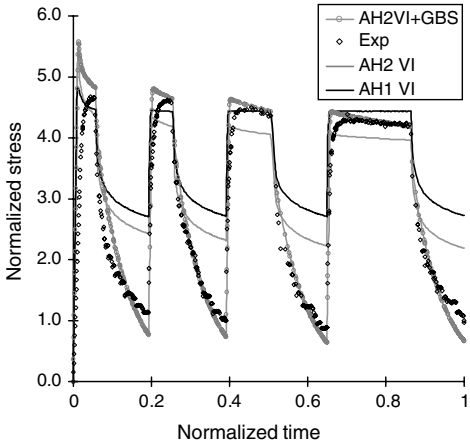

(e) $T = 1561C$, $\dot{\varepsilon} = 2.06E-5\,\mathrm{s}^{-1}$

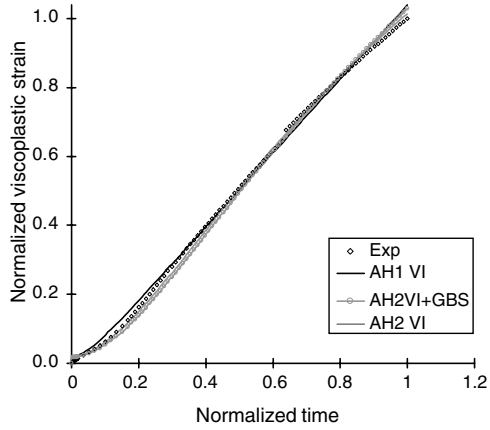

(f) $T = 1494C$, $\sigma = 60.1MPa$

Fig. 6. Identification of the AH-like models, $\varepsilon_M \approx 6.5\%$. Figures (a)–(e) are strain hardening tests with stress relaxation steps and (f) is a creep test.

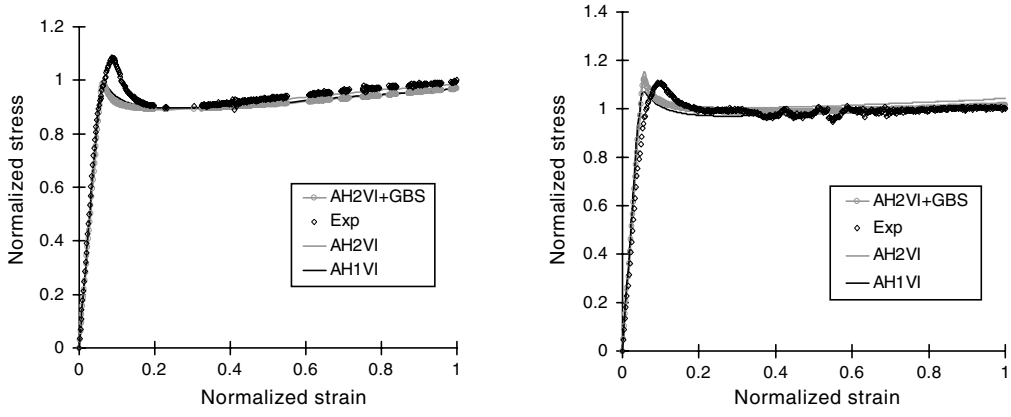

(a) $T = 950C$, $\dot{\varepsilon} = 2.22E-5\,\mathrm{s}^{-1}$ (b) $T = 1150C$, $\dot{\varepsilon} = 2.27E-5\,\mathrm{s}^{-1}$

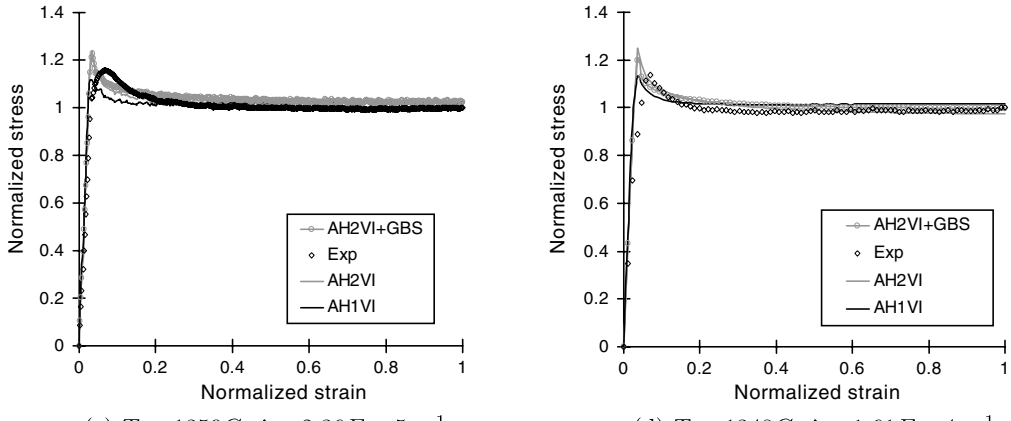

(c) $T = 1350C$, $\dot{\varepsilon} = 2.36E-5\,\mathrm{s}^{-1}$ (d) $T = 1348C$, $\dot{\varepsilon} = 1.61E-4\,\mathrm{s}^{-1}$

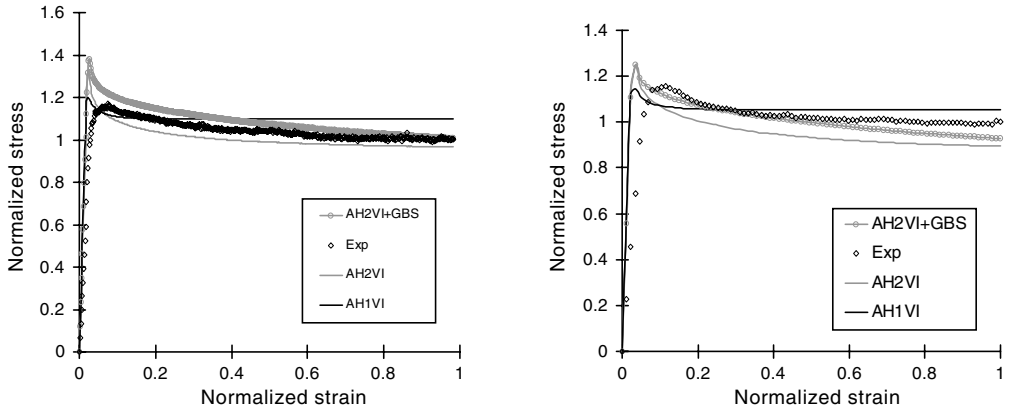

(e) $T = 1570C$, $\dot{\varepsilon} = 2.70E-5\,\mathrm{s}^{-1}$ (f) $T = 1571C$, $\dot{\varepsilon} = 1.57E-4\,\mathrm{s}^{-1}$

Fig. 7. Simulation of the constant strain rate tests with the AH-like models, $\varepsilon_M \approx 7.0\%$.

appearance of textures. Moreover, the internal stress only roughly describes the interaction of forest dislocations and we are not able to distinguish the contribution of a given slide system to the viscoplastic flow and even less to the internal stress, since we have only considered one slip system.

The use of a polycrystalline approach allows the extension of the previous results introducing a distribution

of crystalline orientations for a representative set of grains in which one considers the contribution of the independent slip systems. In Section 4, we recall the principle of the polycrystalline approach and we see how the AH-like model with two internal variables is used to describe the viscoplastic strain rate on a given slip system and consequently how the scope of the previous results is extended. As all the deformations are supposed *a priori* to be intragranular, the grain boundary diffusion mechanism which amounts to grain boundary sliding shall be disregarded. Hence, we focus on the moderate temperature range, i.e. $T \leqslant 1200$ °C.

4. Polycrystalline approach

In order to define more accurately the internal variables corresponding to the dislocation densities and the internal stress and hence the interaction between forest dislocations of various glide systems, we choose to use a polycrystalline approach. For its relative simplicity, we use the polycrystalline model developed by Pilvin [23] and Cailletaud [24].

4.1. Local behavior

Hereafter we define the local behavior within a phase. As the material is supposed monophasic, a phase is a set of grains with the same cristalline orientation.

Each glide system is characterized by its Schmid's tensor $\boldsymbol{m}_s$ with:

$$\boldsymbol{m}_s = \frac{1}{2}(\boldsymbol{l}_s \otimes \boldsymbol{n}_s + \boldsymbol{n}_s \otimes \boldsymbol{l}_s), \quad \boldsymbol{l}_s = \frac{\boldsymbol{b}_s}{\mathtt{b}_s}, \tag{31}$$

where $\boldsymbol{n}_s$ is the normal of the slip plan s.

The contribution of a glide system (s) to the plastic strain $\boldsymbol{\varepsilon}^{\mathrm{p}}$ is given by:

$$\dot{\boldsymbol{\varepsilon}}^{\mathrm{p}} = \sum_{s\in S} \boldsymbol{m}_s \dot{\gamma}_s. \tag{32}$$

In order to model the kinetic of γ_s, we use the system called above AH model (2 i.v.) described by Kubin and Estrin [25]:

$$\frac{\mathrm{d}X_s}{\mathrm{d}\gamma^s} = q\left(- c_1\sqrt{Y_s} - c_3 X_s + c_4 \frac{Y_s}{X_s}\right), \tag{33}$$

$$\frac{\mathrm{d}Y_s}{\mathrm{d}\gamma^s} = \left(c_1\sqrt{Y_s} - c_2 Y_s + c_3 X_s\right). \tag{34}$$

Then we are able to compute the shear strain:

$$\dot{\gamma}^s = \zeta\rho_{\mathrm{m}}\left(\frac{\tau_v}{\tau_{\mathrm{i}}}\right)^m \mathrm{sgn}(\tau_s), \tag{35}$$

$$\tau_v = \max(0; |\tau_s| - \tau_{\mathrm{i}}), \tag{36}$$

where τ_s is the shear stress of the glide system (s).

The computation of the internal stress is complex. As a matter of fact, it takes into account the interactions of dislocations with each others hence the glide system interactions. We introduce a hardening matrix $\boldsymbol{A}$ and write:

$$\tau_{\mathrm{i}} = \tau_0 + \alpha\mu\mathtt{b}\sqrt{\sum_{r\in S} A_{rs}\rho_r}, \tag{37}$$

where τ_0 is the critical shear stress. The hardening matrix $\boldsymbol{A}$ can be written $A_{rs} = h_{\mathrm{lat}} + (1 - h_{\mathrm{lat}})\delta_{rs}$. Setting $h_{\mathrm{lat}} = 1$, we have, with the unity matrix, the Taylor's formulae [26]:

$$\tau_{\mathrm{i}} = \tau_0 + \alpha\mu\mathtt{b}\sqrt{\sum_{r\in S} \rho_r}. \tag{38}$$

If $h_{\mathrm{lat}} = 0$, there is no interaction between the glide systems. The hardening within a glide system is only dependent on its dislocation density. Since we are not able to observe this phenomenon, h_{lat} is a parameter to identify. Finally, according to [17] $\alpha = 1.48/[2\pi(1 - \nu)]$.

4.2. Localization

From the mechanical variables $(\boldsymbol{\sigma}, \boldsymbol{\varepsilon}, \boldsymbol{\varepsilon}^{\mathrm{p}})$ computed for each phases we now determine the macroscopic behavior of the representative elementary volume characterized by $(\boldsymbol{\Sigma}, \boldsymbol{E}, \boldsymbol{E}^{\mathrm{p}})$. It amounts to computing spatial means of $(\boldsymbol{\sigma}, \boldsymbol{\varepsilon}, \boldsymbol{\varepsilon}^{\mathrm{p}})$ on the REV, which we consider as a set of phases with the same function of cristalline orientation:

$$\boldsymbol{\Sigma} = \sum_{g\in G}(f_g\boldsymbol{\sigma}), \tag{39}$$

$$\boldsymbol{E} = \sum_{g\in G}(f_g\boldsymbol{\varepsilon}). \tag{40}$$

The localization law is set considering every grain as the same ellipsoid:

$$\boldsymbol{\sigma} = \boldsymbol{\Sigma} + \mathscr{C}(\boldsymbol{I} - \mathscr{S})(\boldsymbol{B} - \boldsymbol{\beta}_g), \tag{41}$$

$$\dot{\boldsymbol{\beta}}_g = \dot{\boldsymbol{\varepsilon}}^{\mathrm{p}} - \Delta(\boldsymbol{\beta}_g - \delta\boldsymbol{\varepsilon}^{\mathrm{p}})\|\dot{\boldsymbol{\varepsilon}}^{\mathrm{p}}\|, \tag{42}$$

where $\boldsymbol{B} = \sum_{g\in G}(f_g\boldsymbol{\beta}_g)$, $\mathscr{C}$: tensor of elastic modulus (isotropic and homogeneous), $\mathscr{S}$: Eshelby's tensor for an ellipsoidal inclusion.

This practical formulation is simpler to use than Berveiller and Zaoui's scheme. Nevertheless, it is necessary to determine the two parameters Δ and δ to satisfy self-consistency. They are identified by finite element analysis since the comparison to the BZ model even with a tangent approach is limited to monotonous behavior. In equiaxial grains, the phases are assumed spheric. The tensors $\boldsymbol{\beta}_g$ and $\mathscr{S}$ are respectively deviatoric and isotropic. Eq. (41) is then written as:

$$\boldsymbol{\sigma} = \boldsymbol{\Sigma} + 2\mu(1 - \beta)(\boldsymbol{B} - \boldsymbol{\beta}_g). \tag{43}$$

4.3. Identification of the model

4.3.1. Identification scheme

The more parameters there are to identify, the harder the identification is. Many parameters can not be deduced from observation, and there are is no proof that there is a unique identification on this database. Therefore a numerical identification is proposed using the Code *SiDoLo*. Let us recall that the aim of this section is to demonstrate the ability of the polycrystalline approach the reproduce the behavior of uranium dioxide.

To simplify this calculation, we only take into account the principal glide plan (1 0 0). Taking secondary plans into account would be made by using different values for τ_0 in Eq. (38) (see [27]).

As the Young's modulus is explicitly used in the localization scheme, we can no longer use an apparent modulus M_a to include the stiffness of the test apparatus. Therefore, we have modified the experimental data in order not to be mislead by the apparatus stiffness and to be consistent with the elastic properties of uranium dioxide. Moreover, we introduce a scalar in the Young's modulus to take into account the mechanical damage:

$$E^{u} = E_0^{u} * (1 - c_d \varepsilon^{\mathrm{vp}}). \tag{44}$$

Finally, since the current homogenization does not include the intergranular sliding, we only consider temperature over the range [950; 1150 °C].

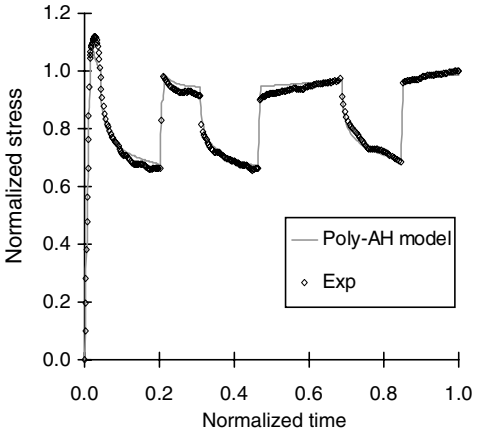

(a) $T = 950C$, $\dot{\varepsilon} = 1.45E-5\,\mathrm{s}^{-1}$

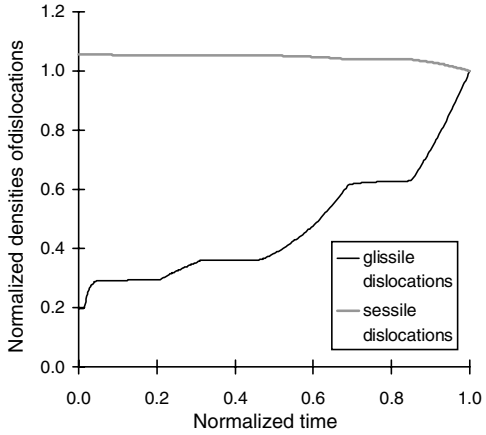

(b) Evolutions of the dislocation densities

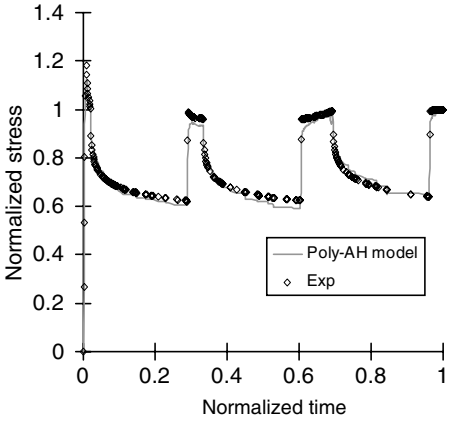

(c) $T = 950C$, $\dot{\varepsilon} = 6.24E-5\,\mathrm{s}^{-1}$

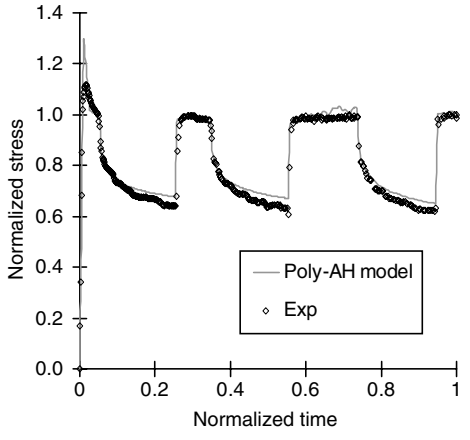

(d) $T = 1150C$, $\dot{\varepsilon} = 2.36E-5\,\mathrm{s}^{-1}$

Fig. 8. Identification of the Alexander and Haasen's model with two dislocation densities in the polycrystalline approach, $\varepsilon_M \approx 6.5\%$.

Table 3
Coefficient of the modified Alexander and Haasen in the polycrystalline formalism

AH-2vi model	Coefficients	Fixed coefficients
q		1.000
m	10.24	
n	5.918	
c_1	9.157	
c_{20}	3.000E3	
c_3	3.144E−7	
c_4	2.987E3	
ρ_{f0} (m^{-2})	2.27E6	
E_0^y (MPa)	2.023E5	
c_d	8.507E−3	
ζ (s^{-1})	2.707E−24	
p	9.084E−2	
pq		9.137E−1
ΔH_0 (J/mol)	5.074E6	
K_{HP} (MPa/$mm^{1/2}$)		6.536E−1
h_{lat}	6.874E−1	
Δ	1.019E4	
δ	7.941E−3	
Number of coefficients	14	3

Table 4
Parameters of the AH-like models

Coefficients	Model-2iv-gbs	Model-2iv	Model-1iv
q	1.000	1.000	
m	9.297	2.960	9.341
n	5.461	3.143	
c_1	1.302E2	16.01	3.334E4
c_{20}	1.605E3	3.128E4	8.435E3
c_3	2.551E−8	2.487E−8	
c_4	6.183E4	1.111E3	
ρ_{f0} (m^{-2})	5.8E10	5.8E10	4.139E9
M_a (MPa)	7.041E4	7.073E4	7.762E3
ζ (s^{-1})	2.691E−4	4.192E−3	
p	7.853E−1	1.478E−2	2.064E−2
pq	8.679E−1	9.137E−1	5.601E−1
ΔH_0 (J/mol)	3.034E5	6.120E6	7.788E5
K_{HP} (MPa/$mm^{1/2}$)	3.772E1	2.03	0
r (mm)	5.967E−5		
α^*	3.229E−2		
ΔH_B (J/mol)	1.621E5		
Number of coefficients	17	14	8

Table 5
Features of the complementary tests used for identification

Test no.	Temperature (°C)	$\dot{\varepsilon}$ (s^{-1})
1	950	6.24E−5
2	1150	2.35E−5
3	1150	6.53E−5
4	1349	2.40E−5

4.3.2. Results

In Fig. 8 we show the identification results of the model for three representative behaviors of the material between 950 and 1150 °C. The corresponding coefficients are reported in Table 3.

4.3.3. Discussion

The model is in good agreement with the experimental data shown in Fig. 8. Furthermore, it is comparable with the identification of the Alexander and Haasen modified model (see Fig. 6). Nevertheless, the evolutions of the forest dislocation densities are different: they are decreasing functions of the strain from 950 °C whereas previously it would occur above 1350 °C. These dislocations have been annealed or become sessile. The introduction of an intergranular hardening and plastic accommodation counteracts this evolution and triggers a positive hardening slope. This highlights the influence of the intergranular hardening – even though the values Δ and δ represent for a weak contribution. In order to check the validity of the self-consistency scheme for the coefficients Δ and δ, a finite element analysis has been performed and will be presented in another article.

Finally, we note that the value of h_{lat} is between 0 and 1, meaning that there are interactions within the glide systems h_{lat}. Since the value of this parameter is neither 0 nor 1, it needs to be identified numerically. Considering coefficients c_i, their values are close to those of the macroscopic model after a correction of the Taylor factor for c_{20} and c_3. However, for c_1 and c_4 the numerical values differ. The kinetics of forest dislocations is slower than the macroscopic while contrary the sessile kinetics is faster. Note that since we cannot prove that this is a unique identification, these results should be considered with prudence.

5. Conclusion

The aim of the present work was to propose an original approach to simulate the non-monotonous viscoplastic behavior of nuclear fuel pellets under nominal and incidental operating conditions. The leading viscoplastic mechanism of UO_2 pellets has been identified and a dislocation based approach has been used to represent it at a local scale. The Alexander and Haasen's model was chosen for its ability to reproduce the yield point as evidenced on strain rate controlled compressive tests. The use of a polycrystalline framework enables the introduction of the crystallographic structure and the grain heterogeneity of UO_2. Therefore we expect good predictive abilities of the present model and an easier extrapolation to the large deformations or to the irradiated behavior. The grain boundary sliding which has

been evidenced for tests performed above 1400 °C has been neglected in the polycrystalline framework, as the data base available for the identification procedure belongs to [950, 1150 °C] temperature range. The effect of mechanical damage on the elastic properties is taken into account. Future work will extend the validity of the model up to 1400 °C.

Acknowledgements

The authors would like to thank Dr A. Mocellin, Dr F. Dherbey and Mr M. Sladkoff (CEA) for providing the mechanical tests and the informations concerning the microstructures.

The help of Professor Ph. Pilvin and Dr L.P. Kubin is also gratefully acknowledged for their contributions to the modeling.

This work is included in Sauter's PhD thesis which was directed by Christian Cunat from the INPL and Sylvain Leclercq from EDF R&D.

References

[1] S. Leclercq, Nucl. Eng. Des. 185 (1998) 221.
[2] J.M. Lefebvre, Contribution à l'étude de la déformation plastique d'une céramique de structure fluorite: le bioxyde d'uranium, PhD thesis, Université de Poitier, 1976.
[3] A.G. Evans, P.L. Pratt, Philos. Mag. 20 (1969) 1213.
[4] D.B. Knorr, R.M. Canon, R.L. Coble, Acta Metall. 37 (1989) 2103.
[5] Y. Chapron, C. Duguay, A. Mocellin, P. Dehault, Programme Flox. Loi de fluage stationnaire de l'UO_2 non dopé et de UO_2 dopé à l'oxyde de chrome au delà de la limite de solubilité: Premières recommandations, Tech. Rep. DTP/SECC/LPCC/NT/97057A, CEA, 1997.
[6] M.F. Ashby, H.J. Frost, Deformation-Mechanism Maps, Pergamon, London, 1982.
[7] R.L. Coble, J. Appl. Phys. 34 (1963) 1679.
[8] C. Herring, J. Appl. Phys. 21 (1950) 437.
[9] M.F. Ashby, R.A. Verrall, Acta Metall. 21 (1973) 149.
[10] J. Lemaitre, J.L. Chaboche, Mécanique des Solides, Dunod, 1985.
[11] L.M. Kachanov, IVZ Acad. Nauk. SSR Otd. Tech. Nauk. 8 (1958) 26.
[12] V. Roque, Caractérisation par méthodes micro-acoustiques de pastilles de dioxyde d'uranium, PhD thesis, Université de Montpellier, 1999.
[13] F. Dherbey, F. Louchet, A. Mocellin, S. Leclercq, Acta Mater. 50 (2002) 1495.
[14] I. Schaeffler, Modélisation du comportement élasto-viscoplastique anisotrope des tubes de gaine du crayon combustible entre zéro et quatre cycles de fonctionnement en réacteur à eau pressurisée, PhD thesis, Université de Franche-Comté, 1997.
[15] H. Alexander, P. Haasen, Solid State Phys. 22 (1968) 27.
[16] J. Rabier, A. George, Rev. Phys. Appl. 22 (1987) 1327.
[17] A. Moulin, M. Condat, L.P. Kubin, Acta Mater. 47 (1999) 2879.
[18] M. Omri, C. Tete, J.P. Michel, A. George, Philos. Mag. A 55 (1987) 601.
[19] Y. Guérin, Tech. Rep. 170, NT SEAMA, 1976.
[20] Y. Estrin, H. Mecking, Acta Metall. 32 (1) (1984) 57.
[21] L.P. Kubin, Private meetings, 2000.
[22] H.S. Kim, Y. Estrin, M.B. Bush, Acta Mater. 48 (2) (2000) 493.
[23] P. Pilvin, Approches multi-échelles pour la prévision du comportement anélastique des métaux, PhD thesis, Paris VI, 1990.
[24] G. Cailletaud, Une approche micromécanique phénoménologique du comportement inélastique des métaux, PhD thesis, Université de Paris VI, 1987.
[25] L.P. Kubin, Y. Estrin, Acta Metall. 38 (1990) 697.
[26] A. Franciosi, Etude théorique et expérimentale du comportement élastoplastique des monocristaux métalliques se déformant par glissement: modélisation pour un chargement complexe quasi-statique, PhD thesis, Université de Paris Nord, 1984.
[27] A. Alamo, J.M. Lefebvre, J. Soullard, J. Nucl. Mater. 75 (1978) 145.
[28] F. Sauter, Comportement viscoplastique du dioxyde d'uranium à haute température, PhD thesis, Institut National Polytechnique de Lorraine, 2001.
[29] C. Vivant-Duguay, Contribution à l'étude du fluage du dioxyde d'uranium. Rôle des activateurs de croissance cristalline, PhD thesis, INSA Lyon, 1998.